

Literature Review

Matthew Gebert

March 18, 2020

Interfacing topological insulators surface states with ferroics

Contents

1	Introduction	3
2	Topological insulator history	3
2.1	History through Hall effects	3
2.1.1	Quantum Hall effect	3
2.1.2	Quantum spin Hall effect	5
2.1.3	Topological insulators	5
2.1.4	Quantum anomalous Hall effect	5
2.2	Relevant theory and phenomena	6
2.2.1	Topological field theory	6
2.2.2	Dirac fermions	6
3	Topological insulator theory	7
3.1	Berry Phase	7
3.1.1	Aharanov–Bohm Effect	8
3.2	Symmetries	8
3.2.1	Time-reversal symmetry	8
3.2.2	Inversion symmetry	8
3.2.3	Particle-hole symmetry	8
3.2.4	Sublattice symmetry	8
3.2.5	Kramers theorem	8
3.3	Topological invariants	8
3.3.1	TKNN invariant	8
3.3.2	Z_2 invariant	8
3.3.3	Z_2 invariant in 3D	9
3.4	Spin-orbit coupling	9
3.4.1	Dresselhaus effect	9
3.4.2	Rashba effect	10
3.5	Hamiltonians of TI Materials	10
3.5.1	HeTe (Mercury Telluride)	10
3.5.2	Bi ₂ Te ₃ (Bismuth Telluride)	10

4 Topological insulator materials	11
4.1 CdTe/HgTe/CdTe quantum wells	11
4.2 Bi _{1-x} Sb _x	12
4.3 {Bi,Sb} ₂ {Se,Te} ₃ family	12
4.3.1 Bi ₂ Te ₃	13
4.3.2 Bi ₂ Se ₃	14
5 Ferromagnetic Insulators	16
5.1 2D FIs	16
5.1.1 Chromium triiodide (CrI ₃)	16
5.1.2 Cr ₂ Ge ₂ Te ₆ (CGT)	17
5.1.3 Magnesium Titinate (MgTiO ₃ , MTO)	18
5.1.4 Other 2D ferromagnetic materials	18
6 TI & FI heterostructures	19
6.1 Theory	19
6.2 Spin Torque	19
6.2.1 Torque	19
6.2.2 Spin Torque Angle - Spin Torque Efficiency	19
6.2.3 Magnetization	19
6.2.4 Critical Current Density	19
6.2.5 Charge Spin Conversion Efficiency	19
6.3 Experiments	19
6.3.1 Conductive films (non-insulating)	19
6.3.2 Insulating Films	20
6.4 Non-TI Devices	20
7 Experimental methods	20
7.1 Synthesis, Growth and Fabrication	20
7.1.1 MBE Growths	20
7.1.2 Doping	20
7.2 Spectroscopic Metrological Methods	21
7.2.1 ARPES	21
7.2.2 Spin polarized STS	22
7.3 Transport Metrological Methods	22
7.3.1 Quantum Oscillations	22
7.3.2 Magnetization	23
8 Related knowledge & concepts	23
8.1 Symmetry	23
8.1.1 Symmetry points	23
8.2 Fine Structure Constant	24
8.3 Hamiltonians of Crystal Lattices	24
9 Quotes	25
10 Questions to Answer	25
11 Bibliography	25

1 Introduction

In the last two decades there has been a vast discovery of new materials that exhibit phenomenal properties interesting for condensed matter physics research. Usually these materials are stumbled upon experimentally, however in the case of topological materials the setting and expectation was purely theoretical.

Topological insulators (TIs) attract interest because of their unique properties related to electronics. 2D and 3D compounds have edge and surface electronic states respectively, and these states exhibit useful properties such as momentum-spin locking (or localised spin densities) and suppressed back-scattering.

These properties may be used for applications like directing currents that are spinful, ie, exerting magnetic fields or used in spintronics, as well as providing currents that are robust with low resistance due to ensured conductivity.

This literature review aims to walk through the basics of TI materials

TO COMPLETE AFTER WRITING REVIEW

2 Topological insulator history

2.1 History through Hall effects

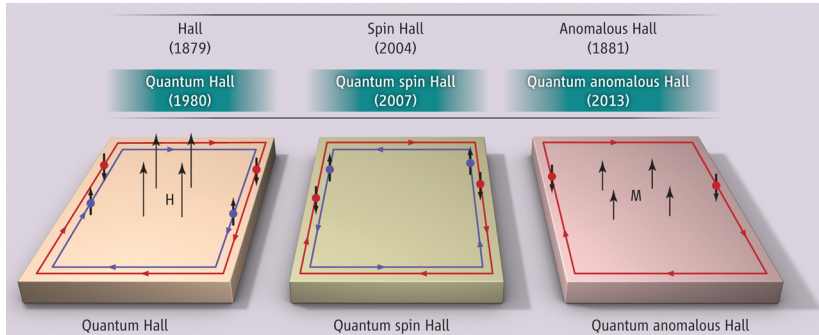


Figure 1: The three QH states discovered thus far^[1]

2.1.1 Quantum Hall effect

The quantum hall effect (QHE) was first discovered in MOSFET¹ transistors 1980^[2], through a 2 dimensional electron gas (2DEG) found at the interface of a bulk semiconductor and the gate oxide.

When introducing a magnetic field to materials, you can produce something called Landau quantisation. You can think of the physical mechanism as the quantisation of cyclotron orbits for charged particles in magnetic fields². This has the effect of creating new bands called "Landau Levels", that each posses large numbers of orbitals. The degeneracy of the level goes as

$$\text{Degeneracy} = \frac{B \times A}{\phi_0} = \frac{B \times A}{h/e} \quad (1)$$

This means for some Fermi energy, that you can choose the magnetic field to appropriate values to fill these Landau levels.

¹Metal-oxide semiconductor field effect transistors

²The reason for cyclotron orbits is due to the single valued electron wavefunction, ie $\oint \vec{P} \cdot d\vec{r} = 2\pi N$

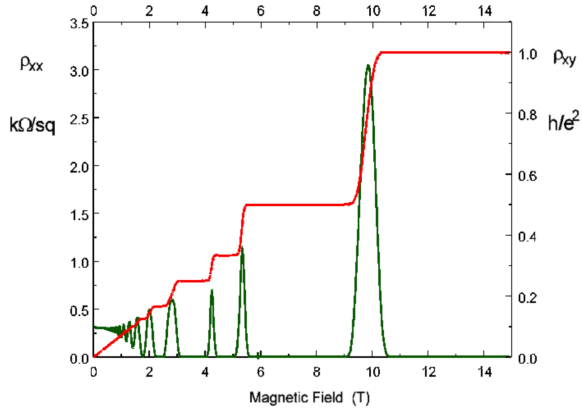


Figure 2: The quantum Hall effect.
Courtesy of D.R. Leadley, Warwick University 1997.

The QHE looks finely tuned, but because of electrons interacting at the edge there is a confinement of edge states^[3]. The edge states dominate transport when the Landau levels of the bulk are filled. Because they are dissipationless, the resistivity ρ_{xx} of the system vanishes, before reaching the next Landau level, where scattering between bulk states can occur again. This is the hallmark^[3] of topological states, where there exists some states between different phases of matter.

The Hall resistivity ρ_{xy} exhibits quantised levels however.

$$\sigma_{xy} = \nu \frac{e^2}{h} \quad (2)$$

Thouless (who later received the noble prize in 2016, before passing away in 2019), Kohmoto, Nightingale, and den Nijs (TKNN)^[4] were interested in gapped bulk systems but with conductive edges and a periodic lattice potential. These systems had been argued for explaining the QHE by Laughlin^[5] and the integer effects had earlier been demonstrated theoretically by Hofstadter's Butterfly^[6]. TKNN recognised that **K** space maps to a non-trivial Hilbert space for the QHE; the space has a topology. This topology can be specified by the integer ν which also corresponds to the hall conductance above in Eq. 2. In particular, their calculations only depended on details of the wavefunctions of the bandstructure.

Show calculation of berry phase of the Bloch wave function calculated around the BZ boundary divided by 2π

What makes this fascinating is that the QHE is a clear example of macroscopic quantum phenomena. Other such phenomena include Bose Einstein Condensation, where many atoms condense into the same uniform quantum state, and superconductivity where the pairing of electrons (Cooper pairs) also produce a new phase of macroscopic quantum behaviour.

For the QHE to occur, the Landau quantisation opens gaps in the band structure of the material, and the chemical potential is situated within this gap. In a classical picture, the boundaries of the material cannot sustain these cyclotron orbits, because of the phase transition to an ordinary insulator, rather than the QHE insulator, and so edge channels open in a **bulk-boundary correspondence**.

Note that the QHE does not preserve **time reversal (TR) symmetry**, as charge carriers experience different forces due to the magnetic field when their direction is inverted. The magnetic field breaks TR symmetry. You can see this in the two degrees of freedom in the system; For an out of plane magnetic field, charge is separated into two lanes, and those channels move a particular direction, ie forward above for electrons, backward below for holes. Reversing the direction of carriers yields the same channels but switched, forward above for holes, backward below for electrons.

³Although unrelated to the Hall effect, get the pun? Haha.

2.1.2 Quantum spin Hall effect

The spin hall was observed in 2004 by Kato *et al.*^[7], where for particular semiconductors a spin density was observed rather than a charge density, like in the regular hall effect. The origins for such an phenomenon are similar to that of the quantum anomalous Hall effect in ferromagnets, sometimes being extrinsic, sometimes intrinsic. Intrinsically, the **Berry curvature** of the electronic valence-band Bloch wave functions result in spin-Hall effect.

The spin Hall insulator was proposed by Zhang's group^[8], where the **Berry phase** is finite implying a finite spin Hall conductivity. While this idea did not “generate spin currents due to an absence of any electrons at the Fermi level”^[9], it allowed further exploration to find it quantised version, a quantum spin Hall (QSH) insulator^[10;11;12].

In a real 1D system with spin, you have a regular four degrees of freedom; Spin can move either direction, and can move forward and backward. This could be separated into two copies of the QH system - spin up moving forward with spin down moving backward at the top, and spin down moving forward with spin up moving backward on the bottom. This is referred to the quantum spin Hall effect (QSHE). But what is the key ingredient that allows this separation of states to occur? In the QHE, it's the magnetic field that breaks time reversal symmetry. For QSH insulators, the essential ingredient is spin orbit coupling (SOC).

An important step made by Kane and Mele^[11] was finding a “topological invariant” to characterise the QSH insulator states using an index. This index is called the Z_2 index. Topological invariants have appeared before. In the QHE, the TKNN invariant μ , where the quantised conductance is proportional to ν . The consequence of the Z_2 index is it maps the parity of the number of times the 1D edge state crosses the Fermi level. An odd parity ensures the existence of an edge state and consequently the phase of a topological insulator. The result is significant in it shows how topological phases exist in band structures of insulators, and do not require external magnetic fields breaking TRS like in the QHE^[9].

Whilst Kane and Mele used their SOC model to investigate the bandgap opening of graphene, SOC is very difficult to experimentally detect in graphene due to the low coupling strength, compared to that of heavier species. Berneveig *et al.*^[10] (Zhang's group) instead proposed a Z_2 model for the band structure of mercury telluride (HgTe). They predicted a CdTe/HgTe/CdTe quantum well would give rise to the QSH effect, when the HgTe layer reached a certain critical thickness. Experimental observation was confirmed soon thereafter by König^[13], who observed a quantised conductivity σ_{xx} of $2e^2/h$, due to two conducting edges. They also observed the thickness dependence.

2.1.3 Topological insulators

By this time theorists (Moore & Balents^[14], Fu, Kane and Mele^[15]) had already leapt forward and predicted 3D systems that would exhibit quantum spin hall effects. It was at this point that the term “topological insulator” was first coined^[14]. This is distinct to the 2D QSH insulators, but analogous in a 3D version. For these systems there was no longer one invariant to determine the topology of a system, but rather 4 separate invariants, for 16 classes of materials. Generally they could be separated into two groups - strong and weak 3D TIs.

The first prediction for a 3D TI was by Fu and Kane^[16]. They predicted that the surface states of bismuth antimony ($\text{Bi}_{1-x}\text{Sb}_x$) could be observed by looking at angle resolved photo emission (ARPES, see 7.2.1). The signature for non-trivial topology was in observing surface states crossing the Fermi energy between two TR-invariant momenta^[16] This was observed in the same system by Hsieh *et al.*^[17].

2.1.4 Quantum anomalous Hall effect

Include some information on the discovery of the QAHE and the AHE, and it's relevance to both magnetic materials in addition to topological phases of matter.

2.2 Relevant theory and phenomena

2.2.1 Topological field theory

In 2001 the QHE state was generalised to a 4D TR-invariant state by Zhang and Hu, and was generalised by to field theory by Bernevig *et al.*. It was also shown later by Zhang how the Z_2 topology could be described in this field theory, and be reduced to the 2D and 3D cases.

Practically this is useful for describing electromagnetic response of TIs and predicting magneto-electric effects, according to Ando's review^[9].

2.2.2 Dirac fermions

Within graphene, mentioned earlier for the Kane and Mele SOC model^[12], the 2D electron gas over the carbon honeycomb lattice creates interesting band structure features called "Dirac cones". The carriers occupying these band structure states behave according to a pseudo-relativistic Dirac equation, behaving differently to that of regular fermions in materials. Their physical behaviour mimics that of highly relativistic situations.

Dirac fermion mass :

Sometimes the charge carriers in graphene are called "massless" Dirac fermions - they behave analogous to relativistic particles with zero rest mass conforming to the Dirac equation^[18]. This result comes from the observation of the fermions having a linear cyclotron mass with energy around the Dirac point's linear dispersion, effectively proving zero dependence on a "rest mass". Instead of their characteristic speed being the speed of light c , the Fermi velocity v_F describes their motion.

Generally in semiconductors and other insulators, the electronic bands either side of the bandgap become quite flat with curvature in momentum space. The important of such features is reflected in the effective mass of carriers as the Fermi energy locally fills states at the band edge. Historically, the effective mass of such carriers is calculated as^[19]

$$m^* = \left(\frac{\partial E^2}{\partial^2 k} \right)^{-1} \quad (3)$$

For parabolic, isotropic bands, a local approximation to the effective mass is:

$$E(\mathbf{k}) = E_0 + \frac{\hbar^2 \mathbf{k}^2}{2m^*} \quad (4)$$

(5)

which satisfies the above calculation. In graphene however, the dispersion equation near the Dirac cones (the K and K' points) are similar to the Dirac equation:

$$E(\mathbf{k}) \approx \hbar v_F \cdot \mathbf{k} \quad (6)$$

If we apply the same effective mass equation, we arrive at:

$$m^* = \left(\frac{\partial v_F \cdot \mathbf{k}}{\partial \mathbf{k}^2} \right)^{-1} \rightarrow \infty \quad (7)$$

If the carriers were really so heavy, conduction would be very restricted in Graphene. Instead, a different method of calculating the effective mass has to be used^[20] avoiding divergence.

$$m^*(E, \mathbf{k}) = \frac{p}{v_g} = h^2 \mathbf{k} \left(\frac{\partial E}{\partial \mathbf{k}} \right)^{-1} \quad (8)$$

$$= \hbar k \frac{1}{v_F} \quad (9)$$

This yields the mass proportional to the linear dispersion, exhibiting relativistic behaviour.

Dirac particles in topological insulators :

As pointed out by Ando^[9], Spin-orbit interactions and 3D “massive” Dirac theory have been known for a long time in Bismuth research, which has also been a playground for its diamagnetism (different to Pauli paramagnetism & diamagnetism). Wolff^[21] showed that a 2 band bismuth model can be transformed into a 4-part Dirac Hamiltonian.

It's interesting that both Bismuth and another semi-metal antimony were used to produce the first 2D TI surface states in $\text{Bi}_{1-x}\text{Sb}_x$ where 2D surface “massless” Dirac systems exist. A distinguishing property of massless Dirac fermions is the Berry phase of π , which provides an absence of backscattering^[22]. The TI surface states consequently electronically protected from some scattering.

3 Topological insulator theory

3.1 Berry Phase

Berry Connection is the bra-ket of a Gradient operator of vector \vec{R} acting on a wavefunction over some path Γ with positions \vec{R} . Physically it is the mechanism from getting one geometric space point to another, ie the change of parameters.

$$\vec{\mathcal{A}}_n(\vec{R}) = i \langle \psi_n(\vec{R}) | \nabla_{\vec{R}} | \psi_n(\vec{R}) \rangle \quad (10)$$

This object has N parts, for each of the vector components. There's a different connection for every eigenstate, of every point in the space. It's a little more subtle than a vector - it transforms under Gauge transformations. For an example wavefunction to include some additional phase factor (i.e. Gauge transformation), the wavefunction transforms as $|\psi'_n(\vec{R})\rangle = e^{-i\beta(\vec{R})} |\psi_n(\vec{R})\rangle$. This results in a change for the Berry connection:

$$\vec{\mathcal{A}}'_n(\vec{R}) = \vec{\mathcal{A}}_n(\vec{R}) + \nabla_{\vec{R}} \beta(\vec{R}) \quad (11)$$

So the “connection” is that it transforms with the gradient of a function, like a vector potential.

Berry Curvature is the consequence or result of going from one set of starting parameters to the same set of parameters over some path (also called a **connection**). You could use the Schroedinger equation to provide a connection. It turns out that through evolution the state can pick-up a phase factor, relative to the original starting state. This phase factor is also known as the Berry phase^[23], and has consequences for the quantum mechanical properties of the system.

The **Berry Phase** is the integral

$$\gamma_n(\Gamma) = \int_{\Gamma} \vec{\mathcal{A}}_n(\vec{R}) \cdot d\vec{R} \quad (12)$$

By changing the gauge of the Berry phase we can notice some properties that shift:

$$\gamma'_n(\Gamma) = \int_{\Gamma} \vec{\mathcal{A}}_n(\vec{R}) \cdot d\vec{R} + \int_{\Gamma} \nabla_{\vec{R}} \beta \cdot d\vec{R} \quad (13)$$

$$\implies \gamma'_n(\Gamma) = \gamma_n(\Gamma) + \beta(R_f) - \beta(R_i) \quad (14)$$

It's not Gauge invariant, which makes it difficult to be useful for different measurements. However, if you begin **AND** end in the same configuration point (ie, a closed loop) then this value is Gauge invariant! This imposes a few restrictions on the system to achieve a result.

- Eigenstates have to be imaginary to achieve a non-zero Berry phase.
- If the path is 1D, then the integration cancels out to result in a zero Berry phase, again.

In 3D systems, the Berry phase over some path Γ enclosing a surface S , then Stokes theorem lets you specify the **Berry curvature**

$$\oint_{\Gamma} \vec{\mathcal{A}}_n \cdot d\vec{R} = \iint_S (\nabla \times \vec{\mathcal{A}}) \cdot d\vec{S} \quad (15)$$

$$\vec{D} = \nabla_{\vec{R}} \times \vec{\mathcal{A}}_n(\vec{R}) \quad (16)$$

3.1.1 Aharonov–Bohm Effect

Todo: Fill out some basic theory and why the Berry phase solves this problem

3.2 Symmetries

3.2.1 Time-reversal symmetry

TODO: explain the role of TR symmetry

3.2.2 Inversion symmetry

Bulk states are spin-degenerate, because of combination of space-inversion symmetry ($E(k, \uparrow) = E(-k, \uparrow)$) and time-reversal symmetry ($E(k, \uparrow) = E(-k, \downarrow)$)^[24]. At the surface however where inversion symmetry is broken, spin-orbit interaction can arise due to asymmetric electric fields and lift the spin degeneracy.

3.2.3 Particle-hole symmetry

TODO: explain the role of particle-hole symmetry

3.2.4 Sublattice symmetry

TODO: explain the role of sublattice symmetry

3.2.5 Kramers theorem

Kramers theorem requires particular points mapped from the BZ (Brouillen zone) to retain spin degeneracy. For $\text{Bi}_{1-x}\text{Sb}_x$, spin states split at the surface by spin-orbit interaction must remain spin-degenerate at four special TR invariant momenta; Γ , and three equivalent M points. Ref in Hsieh *et al.*^[24].

3.3 Topological invariants

3.3.1 TKNN invariant

A detailed calculation for the TKNN invariant will be added in the future.

Simon first showed^[25] that the Berry phase is significantly related to the TKNN topological invariant.

3.3.2 Z_2 invariant

A detailed calculation for this invariant will be added in the future.

3.3.3 Z_2 invariant in 3D

A detailed calculation for this invariant will be added in the future.

- (1;000) - Dirac cone is centred on the $\bar{\Gamma}$ point.

3.4 Spin-orbit coupling

Spin-orbit coupling (SOC) is coupling of both spin and orbital angular momentum properties of particles. Spin provides a magnetic moment, and the motion of the charged electron through its orbital angular momentum also provides a magnetic moment. From the electrons point of view, it can be considered to be the interaction of the electron's spin with the orbital motion of the nucleus, or through a crystal with a periodic potential.

Llewellyn Thomas derived the spin-orbit energy splitting for the hydrogen atom in 1926^[26;27]. You can derive the SOC from the Dirac equation for a spin $\frac{1}{2}$ particle in the presence of an electromagnetic field (ie, proton for hydrogen atom).

$$(E - mc^2) \psi = \left(\frac{p^2}{2m} - \frac{p^4}{8m^3c} + V - \frac{\hbar}{4m^2c^2} \frac{\partial V}{\partial r} \frac{\partial}{\partial r} + \frac{1}{2m^2c} \frac{1}{r} \frac{\partial V}{\partial r} \mathbf{S} \cdot \mathbf{L} \right) \psi \quad (17)$$

The first and third terms are the same as the non-relativistic Schrodinger equation, the second term is the relativistic correction, and the last term is the spin-orbit coupling.

You may also see the SOC represented by Hamiltonian terms such as

$$H_{SO} \propto \boldsymbol{\sigma} \cdot (\vec{\mathbf{E}} \times \vec{\mathbf{p}}) \quad (18)$$

where $\boldsymbol{\sigma}$ are the Pauli matrices, $\vec{\mathbf{E}}, \vec{\mathbf{p}}$ are the external electric field and momentum operator respectively. You can think of the momentum of the electron moving through the electric field as inducing a magnetic field interaction with the spin.

This coupling causes splitting, similar to Zeeman splitting, of electronic energy levels. For different atoms, the SOC is different, with the trend that heavier atoms have a larger SOC^[28].

Add diagram of SOC strength of different atomic species

Within materials, SOC doesn't break time-reversal symmetry like magnetic field does for the QHE, but it can lead to the QSHE, where electrons differentiated by their spin move in opposite directions. Physical effects of SOC in most solid state materials typically result in the Rashba effect or the Dresselhaus effect^[29]

3.4.1 Dresselhaus effect

The SOC for Bloch electrons (crystalline solid state) was first noted by Elliot and Dresselhaus^[30]. Dresselhaus in particular demonstrated the SOC splitting of atomic orbitals could alter cyclotron resonance spectra in semiconductors, and went onto study type III-V and II-VI semiconductor structures in the early 1950's. The Dresselhaus effect occurs in crystals with bulk inversion asymmetry.

Inversion symmetry is when the crystal is symmetric under inversion, from some lattice point from the origin). The breaking of inversion symmetry (inversion asymmetry) is usually important in allowing non-linear effects to take place in materials, otherwise even harmonics of wave functions become suppressed. This includes materials that allow high harmonic generation, such as in ultra-fast femtosecond pulses^[31].

Practically, the fact that net electric fields exist within crystals for particular crystal directions gives rise to spin-orbit interactions.

3.4.2 Rashba effect

Rashba studied a different type of crystal to Dresselhaus, known as a “wurtzite structure” in the late 1950’s. His paper with Sheka demonstrated linear dispersion relationships near the Γ point. This paper (hard to come by online due to lack of translation and availability in the Soviet Union) is translated to English and included in Bihlmayer *et al.*^[30]. The Rashba effect occurs in crystals also with net electric field; this one is due to structural inversion asymmetry, rather than bulk asymmetry. In particular systems such as those with uniaxial symmetry (in one axis only) such as the hexagonal crystals of cadmium-sulphur and cadmium-selenide where it was originally found by Rashba and Sheka.

Rashba-Edelstein Effect in Ferromagnetic Materials Todo: discuss some results of the Rashba effect in magnetic materials.

- <https://doi-org.ezproxy.lib.monash.edu.au/10.1016%2F0038-1098%2890%2990963-C>
- <https://doi-org.ezproxy.lib.monash.edu.au/10.1038%2Fnphys1362>
- <https://www-nature-com.ezproxy.lib.monash.edu.au/articles/nature13534>
- <https://advances.sciencemag.org/content/5/8/eaaw3415>
- https://tms16.sciencesconf.org/data/pages/TI_lecture2.pdf
- <https://arxiv.org/pdf/1401.0848.pdf>

3.5 Hamiltonians of TI Materials

The following models from Qi & Zhang^[32] are formed for QSHE by a Hamiltonian that is a Taylor expansion in the wavevector \mathbf{k} of interactions between highest and lowest conduction bands.

3.5.1 HeTe (Mercury Telluride)

$$H(\mathbf{k}) = \epsilon(k)\mathbb{1} + \begin{pmatrix} M(k) & A(k_x + ik_y) & 0 & 0 \\ A(k_x + ik_y) & -M(k) & 0 & 0 \\ 0 & 0 & M(k) & -A(k_x + ik_y) \\ 0 & 0 & -A(k_x + ik_y) & -M(k) \end{pmatrix} \quad (19)$$

with

$$\epsilon(k) = C + Dk^2, M(k) = M - Bk^2 \quad (20)$$

Here the upper 2x2 block describes the spin-up electrons in the s-like E1 conduction and p-like H1 valence bands. The lower 2x2 block describes the spin-down electrons in those same bands.

ϵ is the unimportant bending of all bands, where $\mathbb{1}$ is the identity matrix. The energy gap between the bands is $2M$, and B describes the curvature of the bands. A incorporates the inter-band coupling at lowest order. $M/B < 0$ has eigenstates of a trivial insulator. $M/B > 0, M$ becomes negative, and solution yields edge states of QSHE. You can also practise doing this with a 2D TI honeycomb lattice to gain explicit understanding like Kane and Mele^[12;11].

Plot and display the eigenstates against momentum

3.5.2 Bi₂Te₃ (Bismuth Telluride)

$$H(\mathbf{k}) = \epsilon(k)\mathbb{1} + \begin{pmatrix} M(\mathbf{k}) & A(k_x + ik_y) & 0 & A_1 k_z \\ A(k_x + ik_y) & -M(\mathbf{k}) & A_1 k_z & 0 \\ 0 & A_1 k_z & M(\mathbf{k}) & -A(k_x + ik_y) \\ A_1 k_z & 0 & -A(k_x + ik_y) & -M(\mathbf{k}) \end{pmatrix} \quad (21)$$

with

$$\epsilon(k) = C + D_1 k_z^2 + D_2 k_\perp^2, M(k) = M - B_1 k_z^2 - B_2 k_\perp^2 \quad (22)$$

Bi_2Te_3 follows a similar model, in the context of bonding and anti-bonding p_z orbitals with both spins. B_1 and B_2 have the same sign, and as before, depending on the sign of M, the bands undergo inversion.

It is essential to be in 3D to be able to construct a single Dirac cone for a 2D surface - the degeneracy of graphene with six Dirac cones makes it clear. The 2D HgTe quantum well at the crossover point $d = d_c$ also has two Dirac cones.

4 Topological insulator materials

4.1 CdTe/HgTe/CdTe quantum wells

The $\{\text{Hg},\text{Cd}\}\text{Te}$ quantum well (QW) was the first successful experiment of a QSH insulator (a 2D TI), with thin layer of HgTe sandwiched between two layers of CdTe (Fig. 3). This system becomes 2D due to quantum confinement from quenching of the out-of-plane direction. Bulk HgTe exhibits a band inversion necessary to observe a QSH effect, whereas CdTe does not. However, HgTe is also a zero-gap semiconductor due to a symmetry protected Γ point. By sandwiching HgTe in CdTe, the slightly larger lattice parameter of CdTe applies a strain on the crystal structure of the thin HgTe when grown the MBE, such that the cubic lattice symmetry is broken and leads to a bandgap opening, becoming a genuine insulator. BHZ predicted that above some critical thickness, the band inversion would be retained and become a TI^[10].

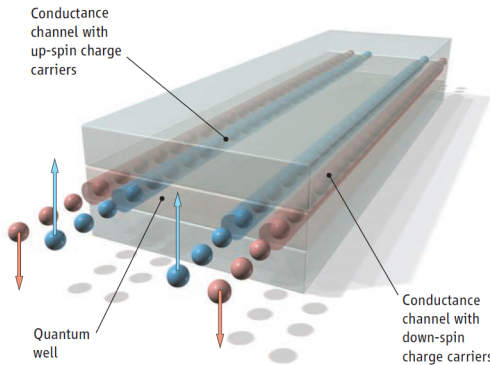


Figure 3: Schematic of CdTe/HgTe QW structures. Devices were patterned into hall bar geometries.

Source: König *et al.*^[13], Science 318

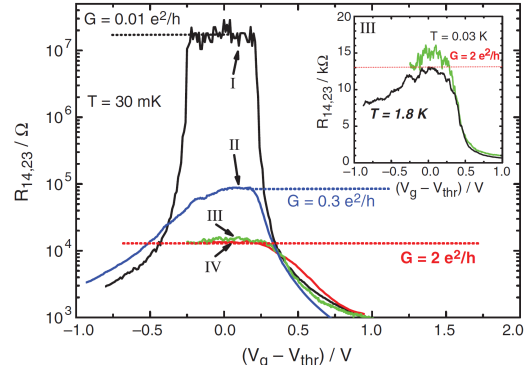


Figure 4: The longitudinal four-probe resistance of various CdTe/HgTe QW structures. HgTe thickness in I is 5.5nm, II,III and IV are 7.3nm. All devices measured at $B=0\text{T}$, $T=30\text{mK}$,

Source: König *et al.*^[13], Science 318

These characteristics were confirmed later by König *et al.*^[13] from the Würzburg group, as shown in Fig. 4. The detected thickness at which the band inversion occurred was at 6.3nm (almost exactly at the prediction of 6.4nm^[10]), where the observation of a quantised conductance became present at low temperatures, previously having diverging resistance. This material only had a bandgap of 10meV resulting from the strain, and so could only be properly measured at sufficiently low temperatures. A quick back of the envelope calculation using $k_B T = \Delta E$ gives a temperature of 116.04 K.

Q: Why was there a lack of band-inversion prior to 6.3nm? As the crystal gets thicker, the less the epitaxial stretching affects the lattice parameters and consequently allows room for band inversion,

whilst maintaining a bandgap? If I get too thick, do I just return to HgTe behaviour which has a closed gap?

4.2 $\text{Bi}_{1-x}\text{Sb}_x$

Bismuth Antimony ($\text{Bi}_{1-x}\text{Sb}_x$) is the first 3D topological insulator discovered^[17], after its prediction well grounded prediction by Fu and Kane^[16]. ARPES was used to confirm the material, as shown in Fig. 6. The theoretical concentrations for which the alloy $\text{Bi}_{1-x}\text{Sb}_x$ becomes a TI are shown in Fig. 5.

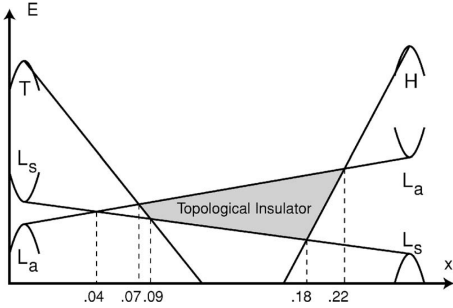


Figure 5: The band energy evolution of $\text{Bi}_{1-x}\text{Sb}_x$ as function of the antimony percentage x .

Source: Fu and Kane^[16], Phys. Rev. B 76, 045302

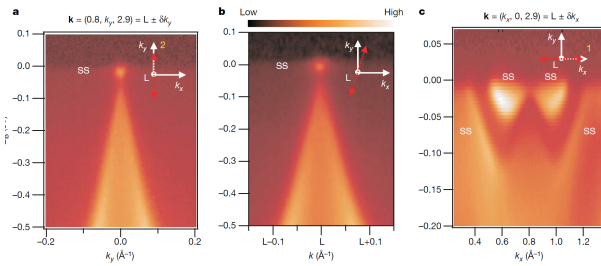


Figure 6: Dirac-like dispersions near the L-point in the bulk BZ in $\text{Bi}_{0.9}\text{Sb}_{0.1}$. **a)** Cut along k_y , **b)** Cut 10° from k_y and **c)** the k_x directions.

Source: Hsieh *et al.*^[17], Nature Vol. 452, 970 (2008)

It is worth noting that $\text{Bi}_{1-x}\text{Sb}_x$ is topologically classed by the Z_2 3D invariant as (1;111). $\text{Bi}_{1-x}\text{Sb}_x$ boasts a high mobility of $\sim 10^4 \text{ cm}^2/\text{Vs}$, whilst the bulk carrier density can be around $\sim 10^{17} \text{ cm}^{-3}$ ^[33]. This sort of mobility makes it easy to study 2D quantum transport according to Ando^[9].

High mobility devices useful for studying because?

Unfortunately, the material's surface states also inherit the strong Rashba-split surface states that are not topological coming from Bismuth; there are 2-4 Fermi-level crossings owing to the Rashba effect, whilst only one topological band (depending on chemical potential), making it complicated to clearly analyse the topological physics present, as discussed in Sec. 7.2.1.

4.3 $\{\text{Bi},\text{Sb}\}_2\{\text{Se},\text{Te}\}_3$ family

Bi_2Te_3 was originally suggested as a candidate without band calculations by Fu and Kane^[16]. However, Zhang *et al.*^[34] filled in the calculations gap, and additionally predicted a whole family of related structures, generalised by the form $A_2B_2B'_1$.

These materials form in a rhombohedral crystal structure, containing 26 A atoms, 26 B atoms, and 20 B' atoms, seen in Fig 7a). However, they're named after their stacked structure of **quintuple layers**, where there are 10 A atoms, 10 B atoms and 5 B' atoms (on average), making a ratio of (2,2,1), or if $B \equiv B'$, (2,3). In the latter case, they are also known as tetradymites.

This class of materials covalently bond within their quintuple layers, but only weakly interact through van der Waals forces, which allows the cleaving between such layers.

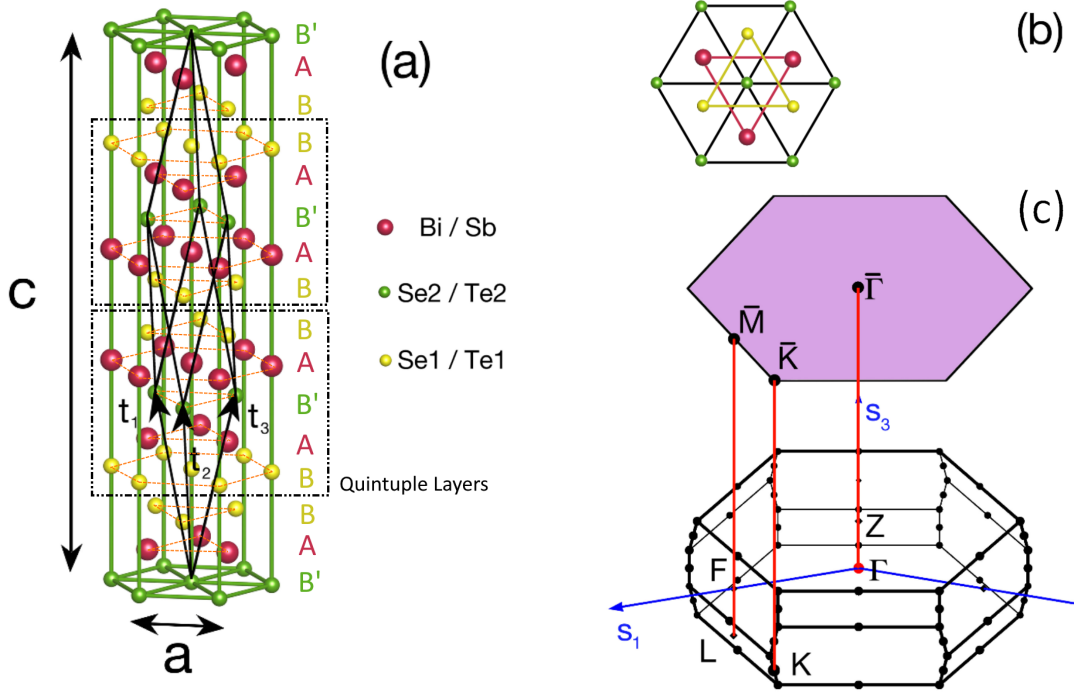


Figure 7: $A_2B_2B'_1$ family. **a)** Rhombohedral unit cell ($c \sim 3$ nm). **b)** Z-axis view of unit cell. **c)** Bulk Brillouin zone projected along the [111] direction (purple shaded area).
Adapted from: Aramberri and Muñoz^[35], Phys. Rev. B 95, 205422 (2017)

The tetradymite members of this family include Bi_2Te_3 , Bi_2Se_3 , and Sb_2Te_3 . Interestingly Zhang's calculations determined Sb_2Se_3 to not be a topological insulator.

Other materials that are tetradymite chalcogenides include Bi_2Te_2Se .

4.3.1 Bi_2Te_3

Bismuth telluride has a much smaller bandgap (0.18eV) than that of Bi_2Se_3 (0.35eV), and consequently is difficult to experimentally isolate the topological surface state^[36].

In a landmark study, Hsieh *et al.* observed the first significant evidence of helical Dirac fermions. They used SR-ARPES (see Sec. 7.2.1), with a double Mott detector to systematically measure all three components of the spin as a function of energy and momentum. Because of the Bi_2Se_3 degenerate bulk conduction band close to the Γ point, there is an extra contribution to the density of states, making it clearer to observe momentum-spin locking (the helical nature) in Bi_2Te_3 . These results are shown in Fig. 8.

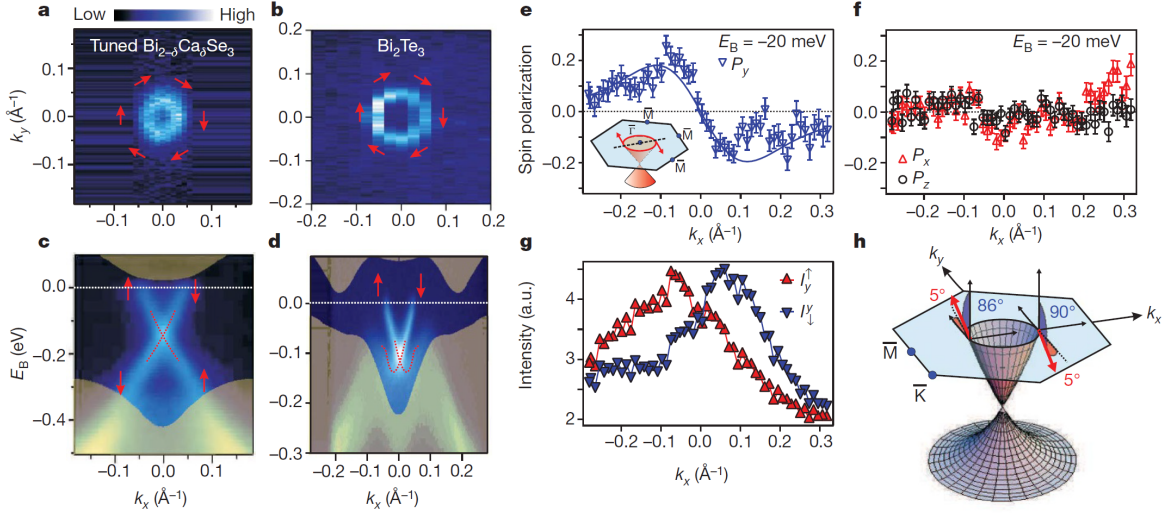


Figure 8: **a,b)** ARPES intensity map of E_F on (111) surface of **a** $\text{Bi}_{2-\delta}\text{Ca}_\delta\text{Se}_3$ and **b** Bi_2Te_3 . **c,d)** Respective ARPES dispersions along the k_x cut. Yellow shaded regions are projections of bulk bands of pure Bi_2Se_3 and Bi_2Te_3 . **e,f)** y component and $\{x,z\}$ components (triangles, circles) of spin polarisation along the $\Gamma - M$ direction, respectively in Bi_2Te_3 . **g)** Spin resolved spectra - counts of different spins at different k_x . Errors attributed to time evolution of the surface band dispersion in Bi_2Te_3 . **h)** Fitted values of spin polarisation vector \mathbf{P} (S_x, S_y, S_z). Angles are shown, contributing to unit vectors $P_{k_x} = (-0.087, -0.996, 0)$ and $P_{-k_x} = (0.087, 0.994, 0.070)$. Errors are of order ~ 10 deg for angles, or ± 0.15 for magnitude.

Source: Hsieh *et al.* Nature 1101, 460 (2009)

4.3.2 Bi_2Se_3

The first observation of the Dirac cone in bismuth selenide (Bi_2Se_3) was reported by Xia *et al.*^[37] Unlike many other topological materials, Bi_2Se_3 is close to the Dirac cone undoped, as shown in Fig. 9a. Normally Bi_2Se_3 is n-type doped due to vacancies or excess selenium^[37] that accumulate through sample growth.

The demonstration of helical Dirac fermions by Hsieh *et al.* mentioned earlier also demonstrated the doped tuning of Bi_2Se_3 to a (relatively) insulating state by using a stoichiometric $\text{Bi}_{2-\delta}\text{Ca}_\delta\text{Se}_3$ ^[36], where Ca acts as a hole donor. Remarkably they are able to demonstrate ARPES data clearly retaining the topological Dirac point at room temperature.

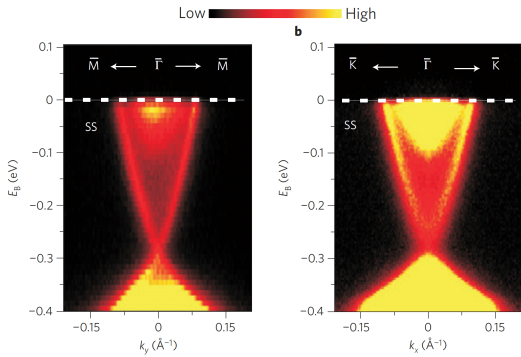
The first significant transport experiment in Bi_2Se_3 by Kim *et al.*^[38] demonstrated a predicted^[39] zero hall coefficient (diverging hall carrier density) at the Dirac point - rather than a zero hall carrier density as one might expect when changing carrier type. This is shown in Fig. 9b. A zero Hall coefficient gives rise to either zero electric field generated or a diverging current density, which is very similar to the behaviour in graphene.

$$R_H = \frac{E_y}{j_x B_z} \quad (23)$$

Kim measured the mobilities of Bi_2Se_3 to be 320-1,500 cm^2/Vs , with the exfoliated flakes possessing n-doped charge densities of $\gtrsim 10^{13} \text{ cm}^{-2}$. This is much greater than the bulk charge density of $\approx 10^{17} \text{ cm}^{-3}$.

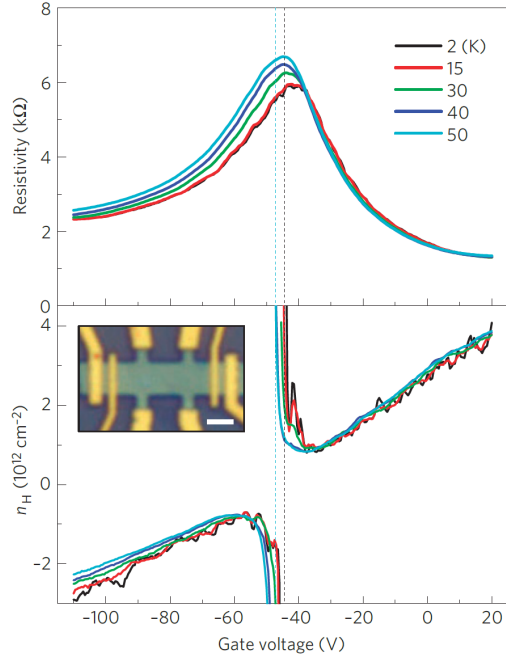
Bi_2Se_3 is classed by the 3D Z_2 invariant as (1;000). Bi_2Se_3 has a bulk bandgap of ~ 0.35 eV. This is a sizeable gap, however unfortunately, even at low temperature (where thermal effects are diminished), the bulk conductivity is quite high due to the small bandgap.

(a) ARPES of Bi_2Se_3 . **a)** From $\Gamma \rightarrow M$ **b)** From $\Gamma \rightarrow K$
 Source: Xia *et al.* Nature Physics 398, Vol 5 (2009)



(b) Bi_2Se_3 longitudinal resistivity ρ_{xx} (top) and sheet carrier density $n = 1/(eR_H)$ (bottom) where R_H is the Hall coefficient and e is the elementary charge.

Source: Kim *et al.* Nature Physics 459, Vol 8 (2012)



It has also been reported that some of these materials (Bi_2Se_3 in particular) undergo surface oxidisation when exposed to ambient (light & air) conditions, degrading their crystal quality and topological properties. The results of Kong *et al.* are shown in Fig. 10^[40]. This has also been reported with other similar materials, such as in the transition metal dichalcogenides (TMDs)^[41].

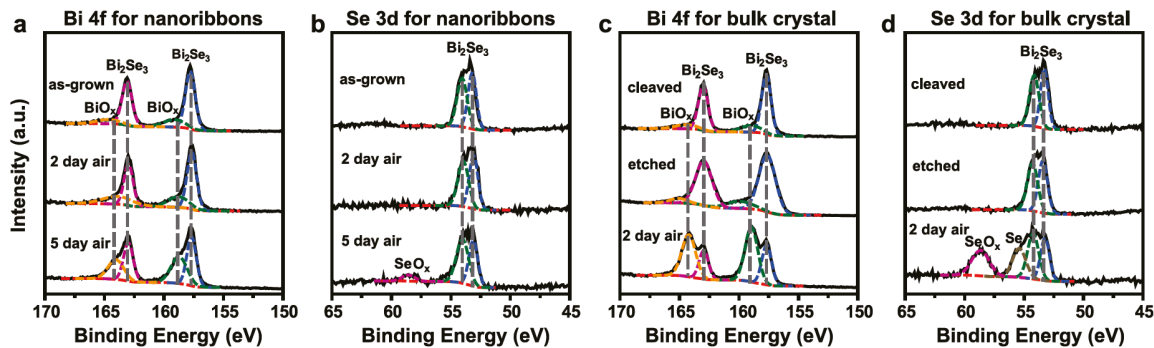


Figure 10: XPS studies on Bi_2Se_3 showing oxidation after exposure to air.

Source: Kong *et al.*, ACS Nano Vol. 5, No. 6, 4698 (2011)

5 Ferromagnetic Insulators

In this section, I will discuss various ferromagnetic insulator (FI) materials that might be used to stack with Bi_2Se_3 . Properties that will matter will include the cleanliness of the interface, the lattice parameters, any resulting strain that might occur, and magnetic properties such as magnetisation amplitude. I will cover new few-layer 2D ferromagnetic insulators that have potential to be used for spin-torque experiments.

FIs are rare, because most magnetic materials that incorporate iron, cobalt or nickel are often conductive. That being said, some 3D FIs have been known for a while, and recently some new FIs that can be exfoliated down to thin flakes have been discovered.

5.1 2D FIs

5.1.1 Chromium triiodide (CrI_3)

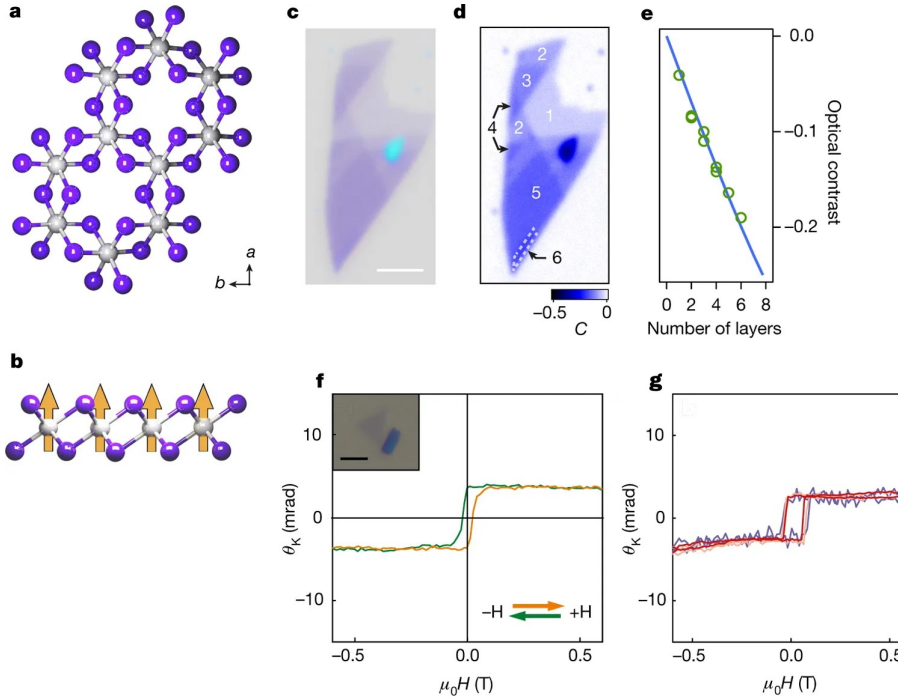
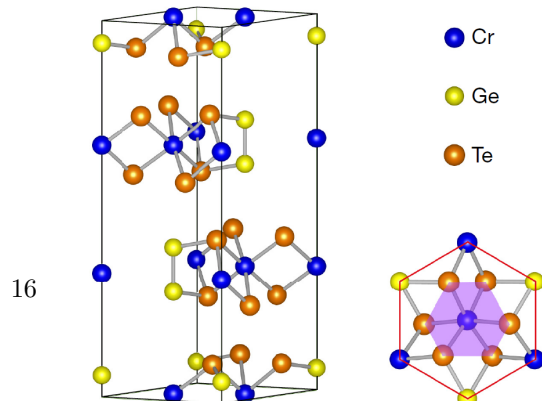


Figure 11: **a)** CrI_3 monolayer atomic lattice. **b)** Out-of-plane view, depicting Ising spin. **c)** Optical image, scalebar $3\mu\text{m}$. **d)** Calculated contrast **e)** Linearity of contrast to thickness. **f)** Kerr signal of monolayer. **g)** Power dependence of Kerr signal taken at powers of $3 \mu\text{W}$ (blue), $10 \mu\text{W}$ (pink), $30 \mu\text{W}$ (red)

Adapted from: Huang *et al.*, Nature Vol. 546, 270 (2017)

CrI_3 was first reported around 2014^[44]. The crystal undergoes a phase change below 220 K from monoclinic to rhombohedral. It has a Curie temperature at 61K in the bulk, and has a resistivity of $900 \Omega\text{cm}$.



Recent reports have demonstrated CrI₃'s ferromagnetic properties persist down to few-layers^[45;46]. Huang *et al.* reports a Curie temperature of 45K for monolayer CrI₃, data shown in Fig. 11. The followup paper shows electrostatic gate control of CrI₃ between ferromagnetic and anti-ferromagnetic states with some spin-locking^[47].

5.1.2 Cr₂Ge₂Te₆ (CGT)

Cr₂Ge₂Te₆ is also a new thin ferromagnetic insulator. It consists of quintuple layers, similar to Bi₂Te₃ or Bi₂Se₃, and is also terminated with hexagonal Te planes (Fig. 12), making it a van der Waals material.

Crystals have been synthesised in bulk before through a flux method, such as demonstrated by Zhang *et al.*^[48], with clear insulating and magnetic properties.

The discovery paper of 2017^[49] shows that bilayers are stable for exfoliation, and magnetic order is found using a scanning Kerr microscope. It was noted that monolayers were thought to be invisible. Whilst the bulk material has a Curie temperature of 61K, the 2D material is less stable, being well defined below 40K. This is very similar to CrI₃. While this is quite novel for investigating low dimensional physics and magnetic-spin effects, this material lacks the high temperature range to be practical around ambient temperatures.

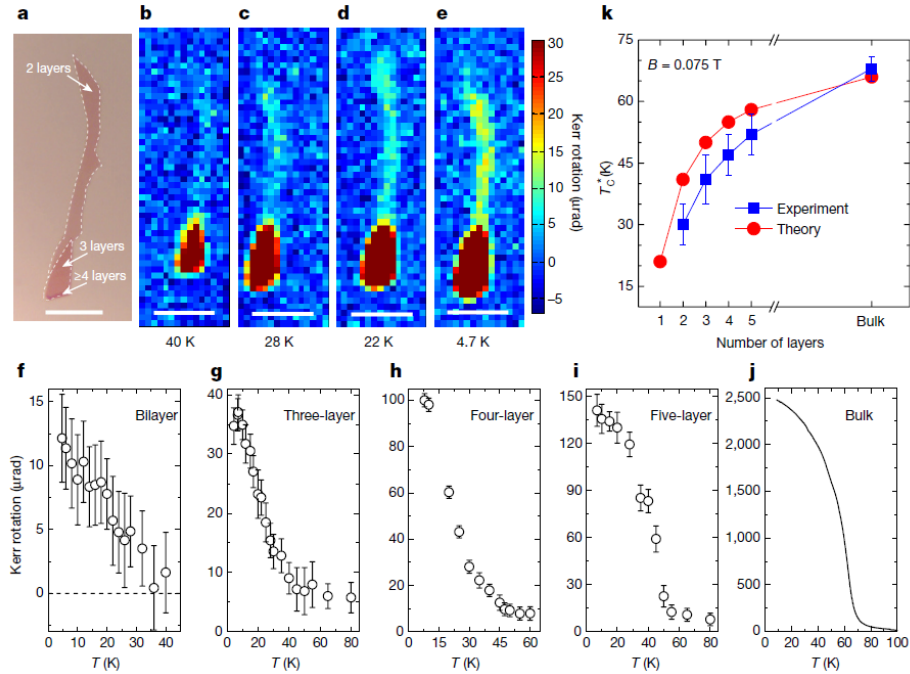


Figure 13: **a)** Microscopy of Cr₂Ge₂Te₆. **b-e)** Appearance of Kerr rotation signal **f-j)** Temperature dependence of Kerr signal in different thicknesses. **k)** Calculations of transition temperatures.

Source: Gong *et al.*, Nature Vol. 546, 265 (2017)

More recent transport data was published by using Pt electrodes, showing the conductivity that appears above 60 K, compared to the massive resistance below^[50]. There are also promising predic-

tions to increase the Curie Temperature of CGT towards liquid nitrogen temperatures, through the use of absorption of gas molecules (NO , NO_2)^[51].

The perpendicular magnetic anisotropy (PMA) is a measure of how strong the magnetic interactions are in the perpendicular direction. This is particularly important for memory or torque devices. For CGT, a PMA energy of 10^5 erg/cm³ is reported^[52].

5.1.3 Magnesium Titinate (MgTiO_3 , MTO)

MTO is another recent addition to thin film ferromagnetic insulator films. Frantti *et al.* reported the stoichiometric material in 2019^[53].

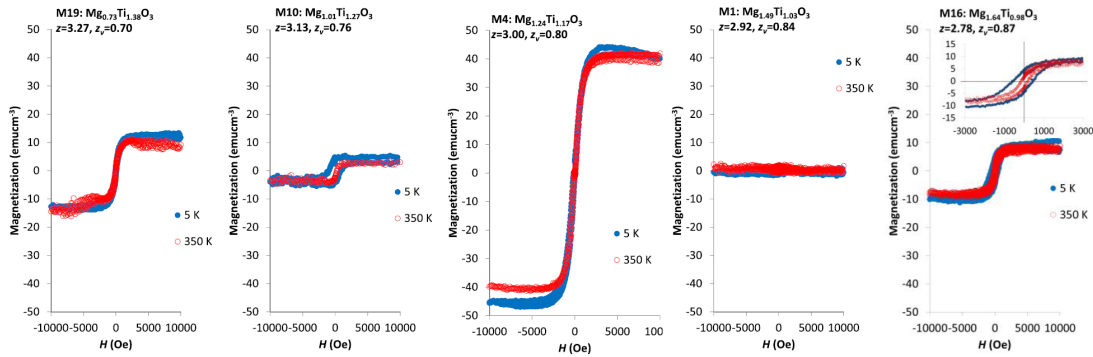


Figure 14: Magnetisation measurements for various mixtures of Mg and Ti in MGO, for two different temperatures. Average valence z and octahedral filling fractions z_v are shown.

Source: Frantti *et al.*, J. Phys. Chem. C 123, 19970 (2019)

MTO has a rhombohedral ilmenite structure, and in this study was grown via a pulsed laser deposition technique to deposit films of thicknesses around 50-60 nm. Across a variety of samples, Frantti saw magnetization swings of up to $\Delta M = 80 \text{ emu cm}^{-3} = 8 \times 10^4 \text{ Am}^{-1}$ (see Fig. 14). A few resistivity measurements of samples were reported, which were 0.07 and 265 MΩ cm, the latter reported to be very typical of most samples.

5.1.4 Other 2D ferromagnetic materials

While an insulator is preferable due to the clear picture expected when interfacing with topological insulator surface states, it's worth noting other 2D ferromagnetic developments. As of 2018, Fe_3GeTe_2 has also been recognised as a 2D van der Waals material possessing ferromagnetism to a much higher Curie temperature (~ 230 K)^[54]. This material also has a much larger PMA than CGT, boasting $\sim 10^7$ erg/cm³.

6 TI & FI heterostructures

6.1 Theory

6.2 Spin Torque

6.2.1 Torque

6.2.2 Spin Torque Angle - Spin Torque Efficiency

6.2.3 Magnetization

Larmor Equation:

$$\vec{T} = \mu_0 \vec{M} \times \vec{H} \quad (24)$$

Torque:

$$\frac{d\vec{L}}{dt} = \vec{T} \quad (25)$$

Gyromagnetic Ratio

$$\gamma \equiv \frac{\mu}{L} \quad (26)$$

Magnetization Change

$$\frac{d\vec{M}}{dt} = \gamma \vec{T} \quad (27)$$

6.2.4 Critical Current Density

6.2.5 Charge Spin Conversion Efficiency

6.3 Experiments

TODO: go through past experiments. Take significant of results, sample fabrication, experimental methodology.

6.3.1 Conductive films (non-insulating)

- (2012) Liu et al. Beta-Ta with CoFeB (Observed Torque, 2.1mT for 0.7mA, Sputtered/evaporated onto surfaces)
- (Apr 2013) Chang et al. Observation of QAHE - Cr0.15(Bi0.1Sb0.9)1.85Te3 - 5 quintuple layers, on SrTiO₃, grown through MBE. Mobilities lower than 1000cm²/Vs. Chromium doping to make ferromagnetic, RHEED, ARPES.
- (Apr 2014) Y. Fan et al. Epitaxial (Bi0.5Sb0.5)2Te3/(Cr0.08Bi0.54Sb0.38)2Te3 bilayer films, 3 & 6 Quintuple layers respectively. AHE. (θ_{SH} reported to be very large??). Look again at device fab.
- (2014) A.R. Mellnik et al. 8nm Bi₂Se₃ and 8nm / 16nm Ni₈₁Fe₁₉ Bilayer (MBE & Sputtering) (Observed Torque Applied, Torque per unit moment T_{parallel} = 2.7 x 10⁻⁵, T_{perp}=3.7 x 10⁻⁵), $\omega_{SH_parallel}=(2.0 \pm 0.4) \times 105/2e \omega^{-1} m^{-1}$ and $\sigma_{SH_perp} = (1.6 \pm 0.2) \times 105/2e \omega^{-1} m^{-1}$
- (2016) P. Li et al. Pt/BaFe₁₂O₁₉ – Torque observed, value not mentioned.

- (Aug 2017) J. Han et al. (MIT & Samarth Grp) - GaAs / Bi₂Se₃(7.4nm)/CoTb(4.6nm)/SiNx(3 nm) - Magnetron and MBE. Critical current density $2.8 \times 10^6 \text{ A/cm}^2$. 0.16 effective SH angle. Large discrepancies noted in this paper. Also searched (Bi, Sb)₂Te₃, and compared to Pt and other heavy metals.
- (Sep 2017) K. Yasuda et al. Cr_x(Bi_{1-y}Sb_y)_{2-x}Te₃/(Bi_{1-y}Sb_y)₂Te₃ - Magnetic non-magnetic heterostructures. Second Harmonic Voltage governed by asymmetric magnon scattering gives incorrect value of CSC (Charge spin conversion efficiency).
- (Nov 2017) Y. Wang et al. **Bi₂Se₃/NiFe Heterostructure**, Describes contamination of BS, 2DEG to the SOT effects from TSS affecting Bi₂Se₃ systems. Also used Bi₂Se₃/Co40Fe40B20, and Bi₂Se₃ (8 QL)/Py(6nm). Growths on Al₂O₃. Used MgO and Al₂O₃ to protect. Also SiO₂ used for Py devices. Iron Milling used with Photolithography.
- (Jul 2018) Khang et al. Bi_{0.9}Sb_{0.1}, 5/10nm Mn0.45Ga0.55 3nm layers
 $\sigma \approx 2.5 \times 10^5 \omega^{-1} m^{-1}$, $\theta_{SH} \approx 52$ and $\theta_{SH} \approx 1.3 \times 10^7 \hbar / 2e\omega^{-1} m^{-1}$
- (Jul 2018) Mahendra DC et al. BixSe(1-x)/Co20Fe60B20 (Magentron Sputtered)
 $\theta_S = 18.62$ (d.c. planar Hall) & 8.67 (ST-FMR) [Si/SiO₂/MgO (2nm)/BixSe(1-x)(tBS nm)/CoFeB(5nm)/MgO(2nm)/Ta(5nm)] tBS=4,6,8,16,40nm
- (Jan 2018) Y. Li et al. Epitaxial (001) SmB₆/Si thin films (50nm +) with MgO(1.5)/CFB(Co40Fe40B20, 1)/ β -W(0.8) – DC Magnetron sputtering / DC&RF magnetron...

6.3.2 Insulating Films

- (2019) P. Li et al. Bi₂Se₃ and FI - BaFe₁₂O₁₉ <https://advances.sciencemag.org/content/5/8/eaaw3415>
- YIG (2016) H. Wang et al. <https://journals-aps-org.ezproxy.lib.monash.edu.au/prl/pdf/10.1103/PhysRevLett.117.076601>

6.4 Non-TI Devices

- (2010) Co layer 0.6nm, with Pt 3nm and AlO_x layers 2nm, transverse magnetic fields. <https://www-nature-com.ezproxy.lib.monash.edu.au/articles/nmat2613?proof=trueMay>

7 Experimental methods

7.1 Synthesis, Growth and Fabrication

TODO: fill in with summary of previous growth methods and experimental methods used for heterostructures.

7.1.1 MBE Growths

7.1.2 Doping

Kim *et al.*^[38] managed to heavily p-dope a sample of Bi₂Se₃ through the use of F4TCNQ molecules, as well as the use of an electrochemical doping with a polymer electrolyte top gate, in order to p-type dope the sample (see Fig. 15). The latter method works by a capacitance between sample surface to induce negatively charged ions. This was necessary to be able to gate the sample near the Dirac point.

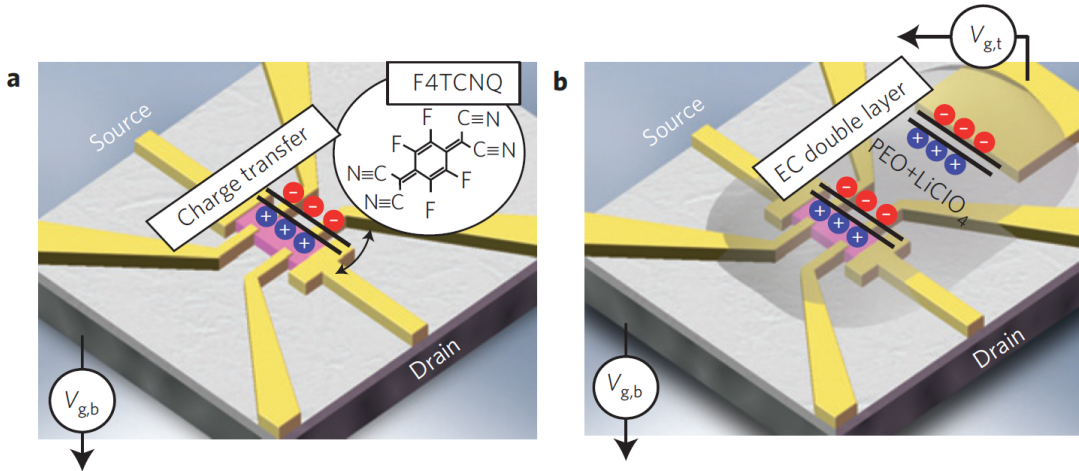


Figure 15: a) P-type doping and gate configuration for charge transfer doping with F4TCNQ molecules b) and polymer electrolyte (PEO + LiClO₄) top gating.

Source: Kim *et al.*^[38], Nature Physics 459, 8 (2012)

Alternatively, Hsieh *et al.*^[36] managed to p-type dope Bi₂Se₃ through the use of an extrinsic molecule nitrogen dioxide (NO₂) in UHV.

7.2 Spectroscopic Metrological Methods

7.2.1 ARPES

For material characterisation, angle resolved photo-emission spectroscopy (ARPES) is a method of resolving the ejection of electrons from a material by high energy photons. Analysis of the momentum of the incident and emission resolve the electronic band structure.

There now exist a variety of different ARPES methods that can be employed in understanding the electronic structure of materials; these include “soft-X-ray ARPES, time-resolved ARPES, spin-resolved ARPES and spatially resolved ARPES”^[55]. The progress fo UV and soft-X-ray synchrotron light sources make it possible to distinguish between bulk and surface states for TI materials. Spin detectors determine the spin state of emitted electrons, allowing insight into spin-textures of surface states. Time-resolved ARPES (using femtosecond pulses) allows observation of “ultrafast electronic dynamics and states above the chemical potential”^[55]. Finally, spatially resolved ARPES can be used to pinpoint sub-micron scale features, particularly if you want to distinguish between phases, or across material gradients (such as gradient MBE growths).

Spin Resolved ARPES The first spin resolved (SR) ARPES that yielded the direct observation of helical spin-polarization was done by Hsieh *et al.*^[24] at the end of 2008 (see Fig. 16), again in Bi_{1-x}Sb_x, followed with more detailed results by Nishide *et al.*^[56].

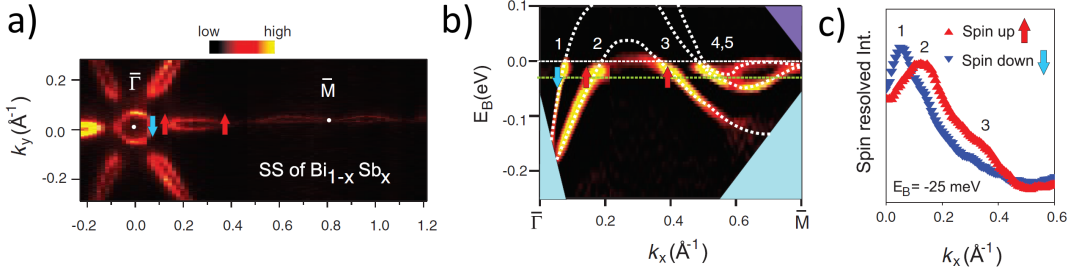


Figure 16: ARPES observation of spin polarised surface states in $\text{Bi}_{1-x}\text{Sb}_x$. **a)** Spin integrated intensity map of $\text{Bi}_{0.91}\text{Sb}_{0.09}$ at E_F . **b)** Surface band-dispersion along the $\bar{\Gamma} \rightarrow \bar{M}$ direction showing 5 Fermi-level crossings. **c)** Spin-resolved momentum distribution curves at binding energy $E_B = -25$ meV, showing band degeneracy.

Source: Hsieh *et al.*^[24], Science Vol. 323, 920 (2009)

In these experiments, topological details could be found by studying the surface band-dispersion and their respective spin polarizations. For example, the fact that there are 5 bands implies that an odd number of Fermi-surfaces enclose the spin-degenerate K points. This gives rise to determining the topological quantum number $\nu_0 = 1$ (0 if even).

However Ando argued that these conclusions were questionable, due to purely relying on states already existing in Bismuth, which did not agree well with theoretical calculations^[9].

A study completed by April 2009 and published in July also by Hsieh *et al.* made the first conclusive observation of helical Dirac fermions in Bi_2Se_3 ^[36]. Here the detection of the spin angular momentum components were measured by the use of two 40-kV Mott detectors.

7.2.2 Spin polarized STS

The first scanning tunnelling spectroscopy (STS) study on $\text{Bi}_{1-x}\text{Sb}_x$ was published in 2009 by Roushan *et al.*^[57] who detected the absence of backscattering even with strong system disorder. By taking fourier transforms of the surface state data they take, they can infer scattering information and lattice information. Combining this with spin-resolved ARPES they could determine the spin dependent scattering probability, and match their STS measurements to 95%. Doing the same with spin-independent scattering yields a match of only 80%.

7.3 Transport Metrological Methods

7.3.1 Quantum Oscillations

Taskin & Ando^[58] used quantum behaviour reported in Bi and $\text{Bi}_{1-x}\text{Sb}_x$ to differentiate between coherent electronic transport (edge states) and incoherent transport within an impurity band. The measurements (along with magnetic & resistivity measurements) where implemented using the “de Haas-van Alphen (dHvA)” effect. To do this, you measure the magnetisation M across magnetic field strengths B. They also measured this quantity for different orientations of the sample, however it is also present in the bare resistivity of the sample.

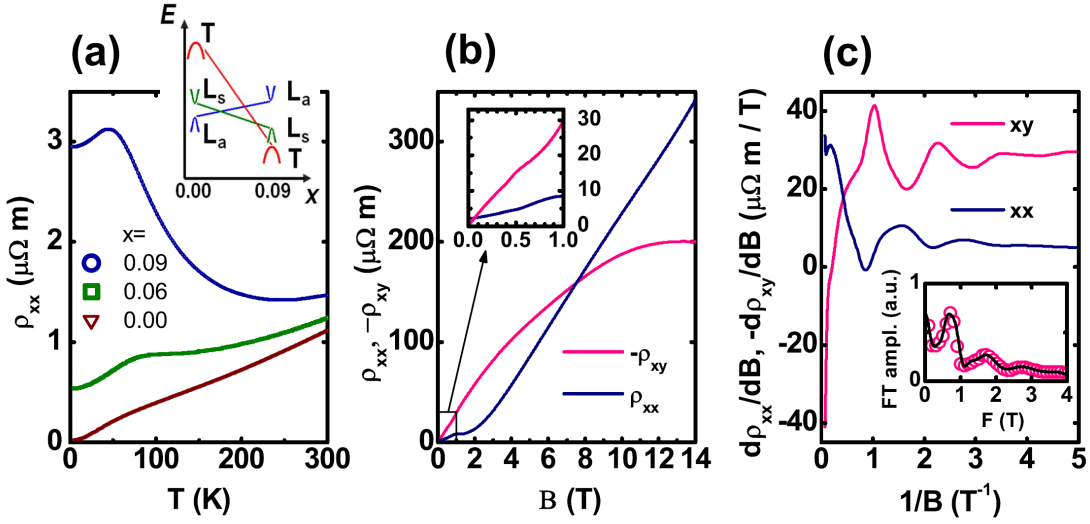


Figure 17: Observation of the quantum oscillations in $\text{Bi}_{1-x}\text{Sb}_x$.

- a) Temperature dependent ρ_{xx} for different x . b) Magnetic field dependent ρ_{xx} and ρ_{xy} for $x=0.09$ @ 1.4K c) Derivatives of b), against $1/B$. Inset shows FT spectrum $-\rho_{xy}$.
 Source: Taskin and Ando^[58] Phys. Rev. B 80, 085303 (2009)

The derivative of the both ρ_{xx} and ρ_{xy} with respect to B , plotted against $1/B$ show Shubnikov-de Haas (SdH) oscillations below 2T field strength, as shown in Fig 17c. This is a quantum effect, and consequently is argued that it comes from a well-defined Fermi surface, not some impurity band which wouldn't be stable. The previous measurements of the resistivity with different doping proportions confirmed the insulating nature of the samples.

7.3.2 Magnetization

Taskin & Ando^[58] measured DC magnetization using a SQUID magnetometer.

8 Related knowledge & concepts

8.1 Symmetry

Symmetry is very important in all physical systems. For example, the order exhibited in crystals can be described through the breaking of the continuous (rotational & translational) symmetry of space. This is due to the electrostatic interactions that cause a periodic lattice. In Magnets, spin space and time reversal symmetry are broken.

8.1.1 Symmetry points

In solid state physics, when observing the reciprocal space for the dispersion relations, there exist particular symmetry points, such as the Γ point, K points, M points and so forth. These have importance in the behaviour of materials due to their propagation vectors through the crystal.

Not sure if this is entirely correct.

General	
Γ	Center of the Brillouin zone
Simple cube	
M	Center of an edge
R	Corner point
X	Center of a face
Face-centered cubic	
K	Middle of an edge joining two hexagonal faces
L	Center of a hexagonal face
U	Middle of an edge joining a hexagonal and a square face
W	Corner point
X	Center of a square face
Body-centered cubic	
H	Corner point joining four edges
N	Center of a face
P	Corner point joining three edges
Hexagonal	
A	Center of a hexagonal face
H	Corner point
K	Middle of an edge joining two rectangular faces
L	Middle of an edge joining a hexagonal and a rectangular face
M	Center of a rectangular face

8.2 Fine Structure Constant

The fine structure constant, also known as Sommerfeld's constant, is the coupling constant " α " that measures the strength of the EM force interacting with light.

Two methods it has been measured by include the anomalous magnetic moment of the electron, a_e , as well as appearing in the Quantum Hall Effect (QHE).

It was originally introduced by Sommerfeld as a theoretical correction to the Bohr model, explaining fine structure through elliptical orbits and relativistic mass-velocity.

8.3 Hamiltonians of Crystal Lattices

Turns out that you can describe the hamiltonian of the electrons in a crystal lattice. For this, there exists first quantisation, second quantisation hamiltonian.

- First quantisation - The classical particles are assigned wave amplitudes. This is "semi-classical" where only the particles or objects are treated using quantum wavefunctions, but environment is classical.
- Second quantisation (Canonical Quantisation, occupation number representation) - The wave fields are "quantized" to describe the problem in terms of "quanta" or particles. This usually means referring to a wavefunction of a state, described the the vacuum state with a series of creation operators to create the current state. Fields are now treated as field operators, similar to how physical quantities (momentum, position) are thought of as operators in first quantisation.

9 Quotes

Finally we introduce the parameter of which all the fuss is about.

R.F. Hofstadter,^[6]

10 Questions to Answer

- SOC - Why only in heavier elements? Explain properly. Also, why think relativistically? Motion of electron means magnetic field observed?
- Spin is in the 2D surface plane of a 3D TI, always perpendicular to that of the momentum - how can I couple a ferromagnetic material if there's no out-of plane?
- ARPES - how can this be used to verify the surface states of TI materials? (and differentiate from the bulk).
- Dirac Cones - why do these only appear in 2D systems.
- Why is spin-polarization called "Helical" spin polarization?

11 Bibliography

- [1] Seongshik Oh. The Complete Quantum Hall Trio. *Science*, 340(6129):153–154, April 2013. ISSN 0036-8075, 1095-9203. doi: 10.1126/science.1237215. URL <http://science.sciencemag.org.ezproxy.lib.monash.edu.au/content/340/6129/153>.
- [2] K. v. Klitzing, G. Dorda, and M. Pepper. New Method for High-Accuracy Determination of the Fine-Structure Constant Based on Quantized Hall Resistance. *Physical Review Letters*, 45(6):494–497, August 1980. doi: 10.1103/PhysRevLett.45.494. URL <https://link.aps.org/doi/10.1103/PhysRevLett.45.494>. Publisher: American Physical Society.
- [3] F. Duncan M. Haldane. Topological Quantum Matter. *International Journal of Modern Physics B*, 32(13):1830004, May 2018. ISSN 0217-9792, 1793-6578. doi: 10.1142/S0217979218300049. URL <https://www.worldscientific.com/doi/abs/10.1142/S0217979218300049>.
- [4] D. J. Thouless, M. Kohmoto, M. P. Nightingale, and M. den Nijs. Quantized Hall Conductance in a Two-Dimensional Periodic Potential. *Physical Review Letters*, 49(6):405–408, August 1982. doi: 10.1103/PhysRevLett.49.405. URL <https://link.aps.org/doi/10.1103/PhysRevLett.49.405>. Publisher: American Physical Society.
- [5] R. B. Laughlin. Quantized Hall conductivity in two dimensions. *Physical Review B*, 23(10):5632–5633, May 1981. doi: 10.1103/PhysRevB.23.5632. URL <https://link.aps.org/doi/10.1103/PhysRevB.23.5632>. Publisher: American Physical Society.
- [6] Douglas R. Hofstadter. Energy levels and wave functions of Bloch electrons in rational and irrational magnetic fields. *Physical Review B*, 14(6):2239–2249, September 1976. ISSN 0556-2805. doi: 10.1103/PhysRevB.14.2239. URL <https://link.aps.org/doi/10.1103/PhysRevB.14.2239>.
- [7] Y. K. Kato, R. C. Myers, A. C. Gossard, and D. D. Awschalom. Observation of the Spin Hall Effect in Semiconductors. *Science*, 306(5703):1910–1913, December 2004. ISSN 0036-8075, 1095-9203. doi: 10.1126/science.1105514. URL <http://science.sciencemag.org/content/306/5703/1910>.

- [8] Shuichi Murakami, Naoto Nagaosa, and Shou-Cheng Zhang. Spin-Hall Insulator. *Physical Review Letters*, 93(15):156804, October 2004. ISSN 0031-9007, 1079-7114. doi: 10.1103/PhysRevLett.93.156804. URL <https://link.aps.org/doi/10.1103/PhysRevLett.93.156804>.
- [9] Yoichi Ando. Topological Insulator Materials. *Journal of the Physical Society of Japan*, 82(10):102001, October 2013. ISSN 0031-9015, 1347-4073. doi: 10.7566/JPSJ.82.102001. URL <http://arxiv.org/abs/1304.5693>. arXiv: 1304.5693.
- [10] B. Andrei Bernevig, Taylor L. Hughes, and Shou-Cheng Zhang. Quantum Spin Hall Effect and Topological Phase Transition in HgTe Quantum Wells. *Science*, 314(5806):1757–1761, December 2006. ISSN 0036-8075, 1095-9203. doi: 10.1126/science.1133734. URL <http://science.sciencemag.org/content/314/5806/1757>. Publisher: American Association for the Advancement of Science Section: Report.
- [11] C. L. Kane and E. J. Mele. Z 2 Topological Order and the Quantum Spin Hall Effect. *Physical Review Letters*, 95(14), September 2005. ISSN 0031-9007, 1079-7114. doi: 10.1103/PhysRevLett.95.146802. URL <https://link.aps.org/doi/10.1103/PhysRevLett.95.146802>.
- [12] C. L. Kane and E. J. Mele. Quantum Spin Hall Effect in Graphene. *Physical Review Letters*, 95(22):226801, November 2005. doi: 10.1103/PhysRevLett.95.226801. URL <https://link.aps.org/doi/10.1103/PhysRevLett.95.226801>.
- [13] Markus König, Steffen Wiedmann, Christoph Brüne, Andreas Roth, Hartmut Buhmann, Laurens W. Molenkamp, Xiao-Liang Qi, and Shou-Cheng Zhang. Quantum Spin Hall Insulator State in HgTe Quantum Wells. *Science*, 318(5851):766–770, November 2007. ISSN 0036-8075, 1095-9203. doi: 10.1126/science.1148047. URL <http://science.sciencemag.org/content/318/5851/766>.
- [14] J. E. Moore and L. Balents. Topological invariants of time-reversal-invariant band structures. *Physical Review B*, 75(12):121306, March 2007. doi: 10.1103/PhysRevB.75.121306. URL <https://link.aps.org/doi/10.1103/PhysRevB.75.121306>.
- [15] Liang Fu, C. L. Kane, and E. J. Mele. Topological Insulators in Three Dimensions. *Physical Review Letters*, 98(10):106803, March 2007. doi: 10.1103/PhysRevLett.98.106803. URL <https://link.aps.org/doi/10.1103/PhysRevLett.98.106803>.
- [16] Liang Fu and C. L. Kane. Topological insulators with inversion symmetry. *Physical Review B*, 76(4):045302, July 2007. doi: 10.1103/PhysRevB.76.045302. URL <https://link.aps.org/doi/10.1103/PhysRevB.76.045302>. Publisher: American Physical Society.
- [17] D. Hsieh, D. Qian, L. Wray, Y. Xia, Y. S. Hor, R. J. Cava, and M. Z. Hasan. A topological Dirac insulator in a quantum spin Hall phase. *Nature*, 452(7190):970–974, April 2008. ISSN 1476-4687. doi: 10.1038/nature06843. URL <http://www.nature.com/articles/nature06843>.
- [18] K. S. Novoselov, A. K. Geim, S. V. Morozov, D. Jiang, M. I. Katsnelson, I. V. Grigorieva, S. V. Dubonos, and A. A. Firsov. Two-dimensional gas of massless Dirac fermions in graphene. *Nature*, 438(7065):197–200, November 2005. ISSN 1476-4687. doi: 10.1038/nature04233. URL <http://www.nature.com/articles/nature04233>. Number: 7065 Publisher: Nature Publishing Group.
- [19] Charles Kittel. Introduction to Solid State Physics, 8th Edition | Wiley. URL <https://www.wiley.com/en-au/Introduction+to+Solid+State+Physics%2C+8th+Edition-p-9780471415268>. Library Catalog: www.wiley.com.
- [20] V. Ariel and A. Natan. Electron effective mass in graphene. In *2013 International Conference on Electromagnetics in Advanced Applications (ICEAA)*, pages 696–698, Torino (Turin), Italy,

September 2013. IEEE. ISBN 978-1-4673-5707-4 978-1-4673-5705-0. doi: 10.1109/ICEAA.2013.6632334. URL <http://ieeexplore.ieee.org/document/6632334/>.

- [21] P. A. Wolff. Matrix elements and selection rules for the two-band model of bismuth. *Journal of Physics and Chemistry of Solids*, 25(10):1057–1068, October 1964. ISSN 0022-3697. doi: 10.1016/0022-3697(64)90128-3. URL <http://www.sciencedirect.com/science/article/pii/0022369764901283>.
- [22] Tsuneya Ando, Takeshi Nakanishi, and Riichiro Saito. Berry’s Phase and Absence of Back Scattering in Carbon Nanotubes. *Journal of the Physical Society of Japan*, 67(8):2857–2862, August 1998. ISSN 0031-9015. doi: 10.1143/JPSJ.67.2857. URL <https://journals.jps.jp/doi/abs/10.1143/JPSJ.67.2857>. Publisher: The Physical Society of Japan.
- [23] M V Berry. Quantal Phase Factors Accompanying Adiabatic Changes. *Proceedings of the Royal Society of London. Series A, Mathematical and Physical Sciences*, 392(1802):14, March 1984.
- [24] D. Hsieh, Y. Xia, L. Wray, D. Qian, A. Pal, J. H. Dil, J. Osterwalder, F. Meier, G. Bihlmayer, C. L. Kane, Y. S. Hor, R. J. Cava, and M. Z. Hasan. Observation of Unconventional Quantum Spin Textures in Topological Insulators. *Science*, 323(5916):919–922, February 2009. ISSN 0036-8075, 1095-9203. doi: 10.1126/science.1167733. URL <http://science.sciencemag.org/content/323/5916/919>.
- [25] Barry Simon. Holonomy, the Quantum Adiabatic Theorem, and Berry’s Phase. *Physical Review Letters*, 51(24):2167–2170, December 1983. doi: 10.1103/PhysRevLett.51.2167. URL <https://link.aps.org/doi/10.1103/PhysRevLett.51.2167>. Publisher: American Physical Society.
- [26] L. H. Thomas. The Motion of the Spinning Electron. *Nature*, 117(2945):514–514, April 1926. ISSN 1476-4687. doi: 10.1038/117514a0. URL <http://www.nature.com/articles/117514a0>. Number: 2945 Publisher: Nature Publishing Group.
- [27] L.H. Thomas. The kinematics of an electron with an axis. *The London, Edinburgh, and Dublin Philosophical Magazine and Journal of Science*, 3(13):1–22, January 1927. ISSN 1941-5982, 1941-5990. doi: 10.1080/14786440108564170. URL <http://www.tandfonline.com/doi/abs/10.1080/14786440108564170>.
- [28] Frank Herman, Charles D. Kuglin, Kermit F. Cuff, and Richard L. Kortum. Relativistic Corrections to the Band Structure of Tetrahedrally Bonded Semiconductors. *Physical Review Letters*, 11(12):541–545, December 1963. ISSN 0031-9007. doi: 10.1103/PhysRevLett.11.541. URL <https://link.aps.org/doi/10.1103/PhysRevLett.11.541>.
- [29] S. Majumdar, H. S. Majumdar, and R. Österbacka. 1.05 - Organic Spintronics. In David L. Andrews, Gregory D. Scholes, and Gary P. Wiederrecht, editors, *Comprehensive Nanoscience and Technology*, pages 109–142. Academic Press, Amsterdam, January 2011. ISBN 978-0-12-374396-1. doi: 10.1016/B978-0-12-374396-1.00023-4. URL <http://www.sciencedirect.com/science/article/pii/B9780123743961000234>.
- [30] G Bihlmayer, O Rader, and R Winkler. Focus on the Rashba effect. *New Journal of Physics*, 17(5):050202, May 2015. ISSN 1367-2630. doi: 10.1088/1367-2630/17/5/050202. URL <http://stacks.iop.org/1367-2630/17/i=5/a=050202?key=crossref.4b499e8c976ab70d1dc90ec00e1cc9ef>.
- [31] Tenio Popmintchev, Ming-Chang Chen, Dimitar Popmintchev, Paul Arpin, Susannah Brown, Skirmantas Ališauskas, Giedrius Andriukaitis, Tadas Balčiunas, Oliver D. Mücke, Audrius Pugzlys, Andrius Baltuška, Bonggu Shim, Samuel E. Schrauth, Alexander Gaeta, Carlos Hernández-García, Luis Plaja, Andreas Becker, Agnieszka Jaron-Becker, Margaret M. Murnane, and

- Henry C. Kapteyn. Bright Coherent Ultrahigh Harmonics in the keV X-ray Regime from Mid-Infrared Femtosecond Lasers. *Science*, 336(6086):1287–1291, June 2012. ISSN 0036-8075, 1095-9203. doi: 10.1126/science.1218497. URL <http://science.sciencemag.org/content/336/6086/1287>. Publisher: American Association for the Advancement of Science Section: Report.
- [32] Xiao-Liang Qi and Shou-Cheng Zhang. The quantum spin Hall effect and topological insulators. *Physics Today*, 63(1):33–38, January 2010. ISSN 0031-9228, 1945-0699. doi: 10.1063/1.3293411. URL <http://physicstoday.scitation.org/doi/10.1063/1.3293411>.
- [33] A. A. Schafgans, K. W. Post, A. A. Taskin, Yoichi Ando, Xiao-Liang Qi, B. C. Chapler, and D. N. Basov. Landau level spectroscopy of surface states in the topological insulator Bi₂Se₃ via magneto-optics. *Physical Review B*, 85(19):195440, May 2012. doi: 10.1103/PhysRevB.85.195440. URL <https://link.aps.org/doi/10.1103/PhysRevB.85.195440>. Publisher: American Physical Society.
- [34] Haijun Zhang, Chao-Xing Liu, Xiao-Liang Qi, Xi Dai, Zhong Fang, and Shou-Cheng Zhang. Topological insulators in Bi₂Se₃, Bi₂Te₃ and Sb₂Te₃ with a single Dirac cone on the surface. *Nature Physics*, 5(6):438–442, June 2009. ISSN 1745-2481. doi: 10.1038/nphys1270. URL <http://www.nature.com/articles/nphys1270>. Number: 6 Publisher: Nature Publishing Group.
- [35] H. Aramberri and M. C. Muñoz. Strain effects in topological insulators: Topological order and the emergence of switchable topological interface states in Sb₂Te₃ / Bi₂Te₃ heterojunctions. *Physical Review B*, 95(20):205422, May 2017. ISSN 2469-9950, 2469-9969. doi: 10.1103/PhysRevB.95.205422. URL <http://link.aps.org/doi/10.1103/PhysRevB.95.205422>.
- [36] D. Hsieh, Y. Xia, D. Qian, L. Wray, J. H. Dil, F. Meier, J. Osterwalder, L. Patthey, J. G. Checkelsky, N. P. Ong, A. V. Fedorov, H. Lin, A. Bansil, D. Grauer, Y. S. Hor, R. J. Cava, and M. Z. Hasan. A tunable topological insulator in the spin helical Dirac transport regime. *Nature*, 460(7259):1101–1105, August 2009. ISSN 1476-4687. doi: 10.1038/nature08234. URL <http://www.nature.com/articles/nature08234>.
- [37] Y. Xia, D. Qian, D. Hsieh, L. Wray, A. Pal, H. Lin, A. Bansil, D. Grauer, Y. S. Hor, R. J. Cava, and M. Z. Hasan. Observation of a large-gap topological-insulator class with a single Dirac cone on the surface. *Nature Physics*, 5(6):398–402, June 2009. ISSN 1745-2473, 1745-2481. doi: 10.1038/nphys1274. URL <http://www.nature.com/articles/nphys1274>.
- [38] Dohun Kim, Sungjae Cho, Nicholas P. Butch, Paul Syers, Kevin Kirshenbaum, Shaffique Adam, Johnpierre Paglione, and Michael S. Fuhrer. Surface conduction of topological Dirac electrons in bulk insulating Bi₂Se₃. *Nature Physics*, 8(6):459–463, June 2012. ISSN 1745-2481. doi: 10.1038/nphys2286. URL <http://www.nature.com/articles/nphys2286>. Number: 6 Publisher: Nature Publishing Group.
- [39] Hideyoshi Fukuyama. Anomalous Orbital Magnetism and Hall Effect of Massless Fermions in Two Dimension. *Journal of the Physical Society of Japan*, 76(4):043711, April 2007. ISSN 0031-9015. doi: 10.1143/JPSJ.76.043711. URL <http://journals.jps.jp/doi/abs/10.1143/JPSJ.76.043711>. Publisher: The Physical Society of Japan.
- [40] Desheng Kong, Judy J. Cha, Keji Lai, Hailin Peng, James G. Analytis, Stefan Meister, Yulin Chen, Hai-Jun Zhang, Ian R. Fisher, Zhi-Xun Shen, and Yi Cui. Rapid Surface Oxidation as a Source of Surface Degradation Factor for Bi₂Se₃. *ACS Nano*, 5(6):4698–4703, June 2011. ISSN 1936-0851. doi: 10.1021/nn200556h. URL <https://doi.org/10.1021/nn200556h>. Publisher: American Chemical Society.

- [41] Jimmy C. Kotsakidis, Quanhui Zhang, Amadeo L. Vazquez de Parga, Marc Currie, Kristian Helmersson, D. Kurt Gaskill, and Michael S. Fuhrer. Oxidation of Monolayer WS₂ in Ambient Is a Photoinduced Process. *Nano Letters*, 19(8):5205–5215, August 2019. ISSN 1530-6984. doi: 10.1021/acs.nanolett.9b01599. URL <https://doi.org/10.1021/acs.nanolett.9b01599>. Publisher: American Chemical Society.
- [42] Peng Li, James Kally, Steven S.-L. Zhang, Timothy Pillsbury, Jinjun Ding, Gyorgy Csaba, Junjia Ding, J. S. Jiang, Yunzhi Liu, Robert Sinclair, Chong Bi, August DeMann, Gaurab Rimal, Wei Zhang, Stuart B. Field, Jinke Tang, Weigang Wang, Olle G. Heinonen, Valentine Novosad, Axel Hoffmann, Nitin Samarth, and Mingzhong Wu. Magnetization switching using topological surface states. *Science Advances*, 5(8):eaaw3415, August 2019. ISSN 2375-2548. doi: 10.1126/sciadv.aaw3415. URL <http://advances.sciencemag.org/content/5/8/eaaw3415>. Publisher: American Association for the Advancement of Science Section: Research Article.
- [43] Hailong Wang, James Kally, Joon Sue Lee, Tao Liu, Houchen Chang, Danielle Reifsnyder Hickey, K. Andre Mkhoyan, Mingzhong Wu, Anthony Richardella, and Nitin Samarth. Surface-State-Dominated Spin-Charge Current Conversion in Topological-Insulator–Ferromagnetic-Insulator Heterostructures. *Physical Review Letters*, 117(7):076601, August 2016. doi: 10.1103/PhysRevLett.117.076601. URL <https://link.aps.org/doi/10.1103/PhysRevLett.117.076601>.
- [44] Michael A. McGuire, Hemant Dixit, Valentino R. Cooper, and Brian C. Sales. Coupling of Crystal Structure and Magnetism in the Layered, Ferromagnetic Insulator CrI₃. *Chemistry of Materials*, 27(2):612–620, January 2015. ISSN 0897-4756, 1520-5002. doi: 10.1021/cm504242t. URL <http://pubs.acs.org/doi/10.1021/cm504242t>.
- [45] Bevin Huang, Genevieve Clark, Efrén Navarro-Moratalla, Dahlia R. Klein, Ran Cheng, Kyle L. Seyler, Ding Zhong, Emma Schmidgall, Michael A. McGuire, David H. Cobden, Wang Yao, Di Xiao, Pablo Jarillo-Herrero, and Xiaodong Xu. Layer-dependent ferromagnetism in a van der Waals crystal down to the monolayer limit. *Nature*, 546(7657):270–273, June 2017. ISSN 1476-4687. doi: 10.1038/nature22391. URL <http://www.nature.com/articles/nature22391>.
- [46] Bevin Huang, Genevieve Clark, Dahlia R. Klein, David MacNeill, Efrén Navarro-Moratalla, Kyle L. Seyler, Nathan Wilson, Michael A. McGuire, David H. Cobden, Di Xiao, Wang Yao, Pablo Jarillo-Herrero, and Xiaodong Xu. Electrical control of 2D magnetism in bilayer CrI₃. *Nature Nanotechnology*, 13(7):544–548, July 2018. ISSN 1748-3395. doi: 10.1038/s41565-018-0121-3. URL <http://www.nature.com/articles/s41565-018-0121-3>. Number: 7 Publisher: Nature Publishing Group.
- [47] Bevin Huang, Genevieve Clark, Dahlia R. Klein, David MacNeill, Efrén Navarro-Moratalla, Kyle L. Seyler, Nathan Wilson, Michael A. McGuire, David H. Cobden, Di Xiao, Wang Yao, Pablo Jarillo-Herrero, and Xiaodong Xu. Electrical control of 2D magnetism in bilayer CrI₃. *Nature Nanotechnology*, 13(7):544–548, July 2018. ISSN 1748-3387, 1748-3395. doi: 10.1038/s41565-018-0121-3. URL <http://www.nature.com/articles/s41565-018-0121-3>.
- [48] Xiao Zhang, Yuelei Zhao, Qi Song, Shuang Jia, Jing Shi, and Wei Han. Magnetic anisotropy of the single-crystalline ferromagnetic insulator Cr₂Ge₂Te₆. *Japanese Journal of Applied Physics*, 55(3):033001, February 2016. ISSN 1347-4065. doi: 10.7567/JJAP.55.033001. URL <http://iopscience.iop.org/article/10.7567/JJAP.55.033001/meta>. Publisher: IOP Publishing.
- [49] Cheng Gong, Lin Li, Zhenglu Li, Huiwen Ji, Alex Stern, Yang Xia, Ting Cao, Wei Bao, Chenzhe Wang, Yuan Wang, Z. Q. Qiu, R. J. Cava, Steven G. Louie, Jing Xia, and Xiang Zhang. Discovery of intrinsic ferromagnetism in two-dimensional van der Waals crystals. *Nature*, 546(7657):265–269, June 2017. ISSN 0028-0836, 1476-4687. doi: 10.1038/nature22060. URL <http://www.nature.com/articles/nature22060>.

- [50] Mark Lohmann, Tang Su, Ben Niu, Yusheng Hou, Mohammed Alghamdi, Mohammed Aldosary, Wenyu Xing, Jiangnan Zhong, Shuang Jia, Wei Han, Ruqian Wu, Yong-Tao Cui, and Jing Shi. Probing Magnetism in Insulating Cr₂Ge₂Te₆ by Induced Anomalous Hall Effect in Pt. *Nano Letters*, 19(4):2397–2403, April 2019. ISSN 1530-6984. doi: 10.1021/acs.nanolett.8b05121. URL <https://doi.org/10.1021/acs.nanolett.8b05121>. Publisher: American Chemical Society.
- [51] Junjie He, Guangqian Ding, Chengyong Zhong, Shuo Li, Dengfeng Li, and Gang Zhang. Remarkably enhanced ferromagnetism in a super-exchange governed Cr₂Ge₂Te₆ monolayer via molecular adsorption. *Journal of Materials Chemistry C*, 7(17):5084–5093, April 2019. ISSN 2050-7534. doi: 10.1039/C8TC05530K. URL <http://pubs.rsc.org/en/content/articlelanding/2019/tc/c8tc05530k>. Publisher: The Royal Society of Chemistry.
- [52] Wen Zhang, Ping Kwan Johnny Wong, Rui Zhu, and Andrew T. S. Wee. Van der Waals magnets: Wonder building blocks for two-dimensional spintronics? *InfoMat*, 1(4):479–495, 2019. ISSN 2567-3165. doi: 10.1002/inf2.12048. URL <http://onlinelibrary.wiley.com/doi/abs/10.1002/inf2.12048>. eprint: <https://onlinelibrary.wiley.com/doi/pdf/10.1002/inf2.12048>.
- [53] Johannes Frantti, Yukari Fujioka, Christopher Rouleau, Alexandra Steffen, Alexander Puretzky, Nickolay Lavrik, Ilia N. Ivanov, and Harry M. Meyer. In Quest of a Ferromagnetic Insulator: Structure-Controlled Magnetism in Mg–Ti–O Thin Films. *The Journal of Physical Chemistry C*, 123(32):19970–19978, August 2019. ISSN 1932-7447. doi: 10.1021/acs.jpcc.9b05189. URL <https://doi.org/10.1021/acs.jpcc.9b05189>. Publisher: American Chemical Society.
- [54] Yujun Deng, Yijun Yu, Yichen Song, Jingzhao Zhang, Nai Zhou Wang, Zeyuan Sun, Yangfan Yi, Yi Zheng Wu, Shiwei Wu, Junyi Zhu, Jing Wang, Xian Hui Chen, and Yuanbo Zhang. Gate-tunable room-temperature ferromagnetism in two-dimensional Fe₃GeTe₂. *Nature*, 563(7729):94–99, November 2018. ISSN 1476-4687. doi: 10.1038/s41586-018-0626-9. URL <http://www.nature.com/articles/s41586-018-0626-9>. Number: 7729 Publisher: Nature Publishing Group.
- [55] Baiqing Lv, Tian Qian, and Hong Ding. Angle-resolved photoemission spectroscopy and its application to topological materials. *Nature Reviews Physics*, 1(10):609–626, October 2019. ISSN 2522-5820. doi: 10.1038/s42254-019-0088-5. URL <http://www.nature.com/articles/s42254-019-0088-5>. Number: 10 Publisher: Nature Publishing Group.
- [56] Akinori Nishide, Alexey A. Taskin, Yasuo Takeichi, Taichi Okuda, Akito Kakizaki, Toru Hirahara, Kan Nakatsuji, Fumio Komori, Yoichi Ando, and Iwao Matsuda. Direct mapping of the spin-filtered surface bands of a three-dimensional quantum spin Hall insulator. *Physical Review B*, 81(4):041309, January 2010. ISSN 1098-0121, 1550-235X. doi: 10.1103/PhysRevB.81.041309. URL <https://link.aps.org/doi/10.1103/PhysRevB.81.041309>.
- [57] Pedram Roushan, Jungpil Seo, Colin V. Parker, Y. S. Hor, D. Hsieh, Dong Qian, Anthony Richardella, M. Z. Hasan, R. J. Cava, and Ali Yazdani. Topological surface states protected from backscattering by chiral spin texture. *Nature*, 460(7259):1106–1109, August 2009. ISSN 1476-4687. doi: 10.1038/nature08308. URL <http://www.nature.com/articles/nature08308>.
- [58] A. A. Taskin and Yoichi Ando. Quantum oscillations in a topological insulator \$Bi_{\{1-x\}}Sb_x\$. *Physical Review B*, 80(8):085303, August 2009. ISSN 1098-0121, 1550-235X. doi: 10.1103/PhysRevB.80.085303. URL <https://link.aps.org/doi/10.1103/PhysRevB.80.085303>.